Experimental Test of the Impulse Approximation in *pd* Inelastic Scattering at 200 MeV*

C. N. BROWN† AND E. H. THORNDIKE
Department of Physics and Astronomy, University of Rochester, Rochester, New York
(Received 12 September 1968)

Inelastic pd interactions have been studied at 200 MeV by bombarding a target of liquid deuterium with a 92% polarized proton beam. The directions and energies of the two scattered protons were measured using thick plastic scintillation counters. Four types of cross sections were studied: (1) the two-proton coincidence rate, $d\sigma/d\Omega_1 d\Omega_2$; (2) the fully differential cross section, $d\sigma/d\Omega_1 d\Omega_2 dE_1$; (3) the single-arm charged-particle yield, $d\sigma/d\Omega_1$; and (4) "singlet deuteron" production. These measured cross sections, and previously reported 145-MeV data of Knuckes *et al.*, are compared with impulse-approximation theories. Our treatment of the spectator model differs from that used previously in that we have treated the kinematics relativistically. The first two cross sections are dominated by quasifree *pp* scattering. Impulse theories which include final-state interaction terms give much better fits to these data than the simple spectator model gives, but there remains an overestimation of the observed cross section in the quasifree *pp* region of about 10%, and the fit in other regions is still qualitative only. The single-arm yield is described very well by a simple sum rule giving the yield as the sum of the free *pp* and *pn* differential cross sections. A final-state-interaction enhancement in the two-proton rate, usually referred to as the "singlet deuteron," was observed in the region of 105° c.m. *pd* elastic scattering having a cross section of 0.3 mb/sr².

I. INTRODUCTION

IN the intermediate energy region, the usual approach to describing nucleon-deuteron scattering is the impulse approximation.[1] This approximation is based on the observation that the radius of the deuteron, 4 F, is larger than the range of nuclear forces, 1.7 F, and hence the nucleons in the deuteron spend a large fraction of the time outside each other's influence. If an incident proton has a wavelength smaller than, say, 1 F, it must scatter essentially independently from the two target nucleons. Hence the interaction of the incident nucleon and the deuteron should be predicted in terms of the well-known nucleon-nucleon amplitudes.[2]

Historically, data on quasifree and slightly inelastic *pd* scattering were collected with the aim of extracting free *np* scattering parameters.[1,3] An example of such a reaction is

$$p+d\rightarrow p+n+p_s \quad \text{(quasifree } pn \text{ scattering)},$$

where the notation p_s indicates a "spectator proton" with momentum typical of the internal momentum of the deuteron, ≈ 50 MeV/c. The impulse-approximation amplitude for this inelastic channel is proportional to the free *pn* scattering amplitude.

We have taken the opposite approach, that of using inelastic *pd* scattering, to study the impulse-approximation description itself. Kuckes *et al.*[4] investigated quasifree *pp* scattering,

$$p+d\rightarrow p+p+n_s, \tag{1.1}$$

and compared the results that they obtained with a simple impulse theory, the spectator model. They noted that the theory predicted the shape of the observed spectra reasonably well but the observed cross section was smaller then predicted. This defect in observed cross sections has also been seen in three-nucleon systems in two recent experiments:

$$p+d\rightarrow d+\gamma+p_s \quad \text{(quasifree } pn \text{ radiative pickup}^5),$$
$$n+d\rightarrow p+n+n_s \quad \text{(quasifree } np \text{ charge exchange}^6).$$

Specifically, we have extended the study of quasifree *pp* scattering away from the quasifree peak and checked more carefully the cross-section defect and the region of applicability of impulse-approximation theories.

This experiment measured the directions and energies of the two final-state protons in (1.1). The cross sections extracted were the double-arm coincidence yield, $d\sigma/d\Omega_1 d\Omega_2$, the shape of the energy spectra of the most differential cross section, $d\sigma/d\Omega_1 d\Omega_2 dE_1$, the total single-arm charged-particle yield, $d\sigma/d\Omega_1$, and the production of the "singlet deuteron." Section II outlines the experimental method and apparatus. In Sec. III, two impulse-approximation descriptions of the reaction are described and in Sec. IV the data reduction and results are presented and compared with the impulse theories. The conclusions reached are discussed in Sec. V.

II. EXPERIMENTAL METHOD

This experiment was performed in the external proton beam of the Rochester 130-in. synchrocyclotron.

* Work supported by the U. S. Atomic Energy Commission. This paper is based on a thesis by C. N. Brown submitted in partial fulfillment of the requirements for the Ph.D. degree at the University of Rochester, 1968.
† Present address: Harvard University, Cambridge, Massachusetts.
[1] R. Wilson, *The Nucleon-Nucleon Interaction* (John Wiley & Sons, Inc., New York, 1963), and references therein.
[2] See review articles (Session B) in Rev. Mod. Phys. **39**, 550 (1967).
[3] E. H. Thorndike, Rev. Mod. Phys. **39**, 513 (1967).
[4] A. F. Kuckes, R. Wilson, and P. F. Cooper, Ann. Phys. (N. Y.) **15**, 193 (1961).
[5] P. F. M. Koehler, K. W. Rothe, and E. H. Thorndike, Phys. Rev. **168**, 1536 (1968).
[6] A. R. Thomas, D. Spalding, and E. H. Thorndike, Phys. Rev. **167**, 1240 (1968).

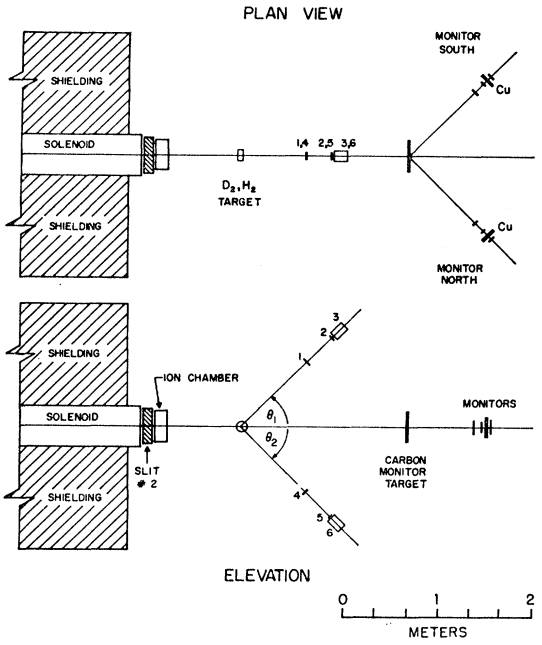

FIG. 1. Plan and elevation views of the experimental setup.

The beam is extracted by scattering from an internal carbon target, thus achieving a vertical polarization of 92%. The last element of the beam transport system, a solenoid magnet, allowed the polarization to be precessed in either sense into the horizontal plane. The final beam had an intensity of 2×10^6 protons/sec over a 2-in. high by 1-in. wide area at the target. The energy at the target was 198 ± 2 MeV with a full width at half-maximum (FWHM) of 14 MeV, and a horizontal and vertical divergence of 5 mrad half-angle.

The target was of standard cryogenic design. Hydrogen or deuterium gas could be liquified at liquid-hydrogen temperatures into a 0.005-in.-thick Mylar cup. The cup had the form of a transverse horizontal cylinder 2 in. in diam by 3 in. long.

Downstream from the main target a $\frac{1}{2}$-in.-thick carbon target was placed in the beam for monitoring purposes. Protons scattered 45° to the left or right from this target were detected in identical three-element scintillation counter telescopes containing $\frac{1}{2}$ in. of copper absorber. The sum of the left and right counts was used as a relative monitor for the hydrogen and deuterium runs. This allowed all normalization to be made relative to the previously measured free pp cross sections at the same angles and energy.[3]

The two proton telescopes are indicated in Fig. 1, a diagram of the experimental setup. Also shown are the solenoid magnet and slits and the downstream monitor. The angles of the two telescopes are specified in polar coordinates θ_1, φ_1, θ_2, and φ_2 with the z axis in the beam direction and the x axis in the vertical direction. For most runs in the experiment the arms were kept in a vertical plane, $\varphi_1=0°$, $\varphi_2=180°$, and the cross sections were studied as a function of the included angle, $\theta_{\rm inc}=\theta_1+\theta_2$.

In each of the two identical telescopes the first plastic scintillation counter was $\frac{1}{16}$ in. thick and the second scintillation counter, the defining counter, was 2 in. in diam by $\frac{1}{16}$ in. thick, situated 50 in. from the target. The third element of each telescope was a 6-in. thick by 3-in.-diam plastic scintillation counter which totally absorbed protons of less than 150 MeV and hence measured their total energy. The outputs of the two total energy counters were fed into analog-to-digital converters which were gated by the fourfold coincidence of the four thin counters. These two outputs, a measure of the proton energies T_1 and T_2, were accepted by an on-line PDP-8 computer, plotted on an X-Y recorder for immediate inspection, and punched on cards for a permanent record. Since the directions and energies of both protons were measured, the kinematics were once overdetermined.

III. IMPULSE APPROXIMATION

Everett[7] has shown that if the T matrix for the total Hamiltonian in pd scattering is expanded in terms of the two-body t matrices, one gets

$$t_{pd}=t_{pp}+t_{np}+t_{pp}gt_{np_1}+t_{pp}gt_{np_2}+t_{np_1}gt_{np_2}+t_{np_1}gt_{pp}+\text{higher terms}, \quad (3.1)$$

where g is the propagator between the subsequent scatterings. Kuckes *et al.*[4] calculated quasifree pp scattering explicitly, considering only the first term in the expansion. Everett[7] used Gammel-Thaler potentials to evaluate double- and triple-scattering terms in (3.1) and he concluded that triple-scattering contributions were the same order of magnitude as double scattering. Cromer[8] extended Kuckes's explicit calculations of the first term in (3.1) and included approximations of some of the double-scattering effects. We shall use Cromer's notation in our calculations.

The spirit of the impulse approximation is to evaluate only the terms which should dominate in a certain kinematic region. The spectator model assumes that the first term in (3.1) dominates quasifree pp scattering and neglects other terms. We write the transition matrix

$$T_{ab}=(\Phi_b^{(-)}, t_{pp}\Phi_a). \quad (3.2)$$

Here Φ_a and Φ_b are the initial and final states, respectively. Using the formulation of the initial and final states used by Cromer[8] and using relativistic phase-space factors, we write the total cross section for reaction (1.1) in terms of the laboratory momenta p_i

[7] A. E. Everett, Phys. Rev. **126**, 831 (1962).
[8] A. H. Cromer, Phys. Rev. **129**, 1680 (1963); A. H. Cromer and E. H. Thorndike, *ibid.* **131**, 1680 (1963).

and total energies E_i:

$$\sigma=\frac{(2\pi)^{-5}}{4mp_0}\int\int\int\frac{d^3p_1}{2E_1}\frac{d^3p_2}{2E_2}\frac{d^3p_3}{2E_3}\delta^4(p_0-p_1-p_2-p_3)\sum_{\text{spin}}|\langle f|T_{ab}|i\rangle|^2. \quad (3.3)$$

The t matrices are related to the nucleon-nucleon c.m. scattering matrix M by

$$t_{pp}(q)=(8m\pi^2E_0)^{1/2}M_{pp}(q), \quad (3.4)$$

where m is the nucleon mass, 939 MeV. Substituting (3.2) and (3.4) in (3.3) and removing the δ function by integrating over d^3p_3 and dp_2 gives the spectator-model prediction for the most differential cross section in quasifree pp scattering:

$$\frac{d\sigma}{d\Omega_1 d\Omega_2 dE_1}=K|f(p_3)|^2\times\tfrac{1}{4}\,\mathrm{Tr}M_{pp}M_{pp}^{\dagger}.$$

Here K is a kinematical factor which has been treated in a relativistically correct way:

$$K=\frac{m(E_0+m)p_1p_2^2}{16\pi^3p_0[p_2(E_2+E_3)-E_2(p_0\cos\theta_2-p_1\cos\theta_{\text{inc}})]}.$$

The nonrelativistic treatment of the kinematics given by Kuckes *et al.*[4] gives a value 5–15% low in the intermediate energy range. $f(p_3)$ is the Fourier transform of the deuteron radial wave function and was derived from a Hulthen wave function for the deuteron.[9]

One can include the effects of the double-scattering terms, approximating them by assuming that only the low-energy s-wave interaction of the nucleons is important in the final state. We have expanded the treatment of the double-scattering terms as given by Cromer[8] and made the resulting equations completely antisymmetric with respect to the two protons in the final state.[10] The predicted cross section for quasifree pp scattering is

$$\frac{d\sigma}{d\Omega_1 d\Omega_2 dE_1}=K\times\tfrac{1}{6}\,\mathrm{Tr}M_{ba}\Lambda_{23}{}^tM_{ba}{}^{\dagger}.$$

Here K is the kinematical factor given above, $\Lambda_{23}{}^t$ is the triplet spin projection operator for nucleons 2 and 3, the proton and neutron originally in the deuteron, and M_{ba} is given by

$$M_{ba}=[f(p_3)+\alpha_3]M_{pp}+[f(p_2)+\alpha_2]M_{np_1}+\eta_{12}[f(p_1)+\alpha_1]M_{np_2}.$$

M_{pp}, M_{np_1}, and M_{np_2} are the two-body scattering matrices expressed in the 8×8 spin space of the three nucleons, and η_{12} is a spin operator for nucleons 1 and 2, $\eta_{12}=\Lambda_{12}{}^t-\Lambda_{12}{}^s$. The α_i give the double-scattering corrections to the spectator-model form factors $f(p_i)$, and a typical term is

$$\alpha_3+s_1\Lambda_{23}{}^s+t_1\Lambda_{23}{}^t+s_2\Lambda_{13}{}^s+t_2\Lambda_{13}{}^t.$$

s_1 is given by

$$s_1=\int\left({}^s\chi_{\omega_{23}}-\frac{\sin\omega_{23}r}{\omega_{23}r}\right)e^{\frac{1}{2}\mathbf{q}_1\cdot\mathbf{r}}\varphi_0(\mathbf{r})d^3r,$$

with

$$\boldsymbol{\omega}_{23}=\tfrac{1}{2}(\mathbf{p}_2-\mathbf{p}_3), \quad \mathbf{q}_1=\mathbf{p}_0-\mathbf{p}_1;$$

the other s_i and t_i have similar forms.[9] ${}^s\chi_\omega$ is the singlet s-wave scattering state constructed from a square well potential whose parameters were adjusted to fit the low-energy scattering parameters. $\varphi_0(\mathbf{r})$ is the deuteron ground-state wave function.

The predictions of this final-state-interaction (FSI) model and the previously described spectator model were evaluated using the values from the 200-MeV phase-shift analysis for the M matrices.[11] The predictions will be compared with experimental measurements in Sec. IV.

IV. DATA REDUCTION AND RESULTS

All rates were corrected for the contributions from random coincidences and target-empty counts. The corrected rates were then used to derive the cross sections $d\sigma/d\Omega_1d\Omega_2$ and $d\sigma/d\Omega_1$. The punched card outputs of the on-line program were used to study the shape of the most differential spectra $d\sigma/d\Omega_1d\Omega_2dE_1$ and the cross section in the region of the singlet deuteron.

$d\sigma/d\Omega_{12}d\Omega$

If we let R_c be the correct coincidence rate between the two telescopes, the cross section is given by

$$\frac{d\sigma}{d\Omega_1d\Omega_2}=\frac{R_cK}{G}, \quad K=\frac{1}{R_H\times\Delta\Omega_2}\left(\frac{d\sigma}{d\Omega}\right)_{pp}\frac{\rho_HN_H}{\rho_DN_D}.$$

The normalization constant K involves the corrected hydrogen rate in one arm times the solid angle of the other arm and also the free pp lab cross section which we take from previously reported measurements.[3] The ratio of densities of nuclei in the liquid H_2 and D_2 targets, ρ_HN_H/ρ_DN_D, is 0.83 ± 0.01.[12] The geometrical factor G corrects for the finite geometry of the experiment.[9]

[9] Further details on this point are contained in a University of Rochester thesis by C. N. Brown (unpublished); copies are available on request.

[10] A. Cromer (private communication).

[11] G. Breit (private communication).

[12] D. B. Chelton and D. B. Mann, Lawrence Radiation Laboratory Report No. UCRL-3421 (unpublished).

TABLE I. Equal-angle results for $d\sigma/d\Omega_1 d\Omega_2$. Errors quoted include normalization errors and statistical errors added quadratically. The predictions were calculated with a 30-MeV energy cutoff on T_1 and T_2. All cross sections are given in mb/sr^2. $\varphi_1=0°$ and $\varphi_2=180°$ for all configurations.

Angle (θ,θ_1)	Experiment	Spectator model	Experiment / Spectator model	FSI model / Spectator model	$\bar{T}_3$ (MeV)
(20, 20)	1.21±0.27	1.96	0.62 ±0.14	0.30	12.8
(25, 25)	2.02±0.34	3.37	0.60 ±0.10	0.42	10.5
(30, 30)	4.44±0.36	7.16	0.62 ±0.05	0.55	7.5
(32.5, 32.5)	7.12±0.35	11.68	0.61 ±0.03	0.63	5.85
(35, 35)	12.0 ±0.63	21.04	0.57 ±0.03	0.71	4.18
(37.5, 37.5)	26.5 ±1.1	42.46	0.625±0.025	0.79	2.60
(40, 40)	67.4 ±1.9	92.31	0.73 ±0.02	0.86	1.33
(41.2, 41.2)	100.6 ±5.2	128.97	0.78 ±0.04	0.88	0.91
(42.2, 42.2)	113.8 ±4.7	156.92	0.725±0.03	0.90	0.69
(43.2, 43.2)	139.0 ±3.4	167.35	0.83 ±0.02	0.91	0.615
(43.5, 43.5)	122.3 ±5.0	165.20	0.74 ±0.03	0.91	0.619
(44.2, 44.2)	122.0 ±6.0	150.77	0.81 ±0.04	0.90	0.703
(45, 45)	91.2 ±3.1	123.18	0.74 ±0.25	0.90	0.914
(46.5, 46.5)	44.1 ±2.1	68.85	0.64 ±0.03	0.89	1.64
(48, 48)	25.4 ±1.4	33.84	0.75 ±0.04	0.90	2.86
(55, 55)	2.90±0.19	1.18	2.46 ±0.16	2.32	16.2
(60, 60)	0.82±0.10	0.13	6.3 ±0.8	8.5	34.7
(65, 65)	0.37±0.06	0.014	26 ±4	37	61.2

The measured and predicted values of $d\sigma/d\Omega_1 d\Omega_2$ for the equal-angle configuration, $\theta_1=\theta_2$, are listed in Table I. The values are plotted in Fig. 2 as a function of the included angle. The data are dominated by the quasifree peak at $\theta_{\text{inc}}=86.4°$; in this region the spectator-model prediction is larger by about 20% than the data. By plotting the ratio of the data to the spectator model and the ratio of the FSI model to the spectator model, as in Fig. 3, the differences are clearly shown. The FSI model gives a much improved fit but the fit is still qualitative only. The 145-MeV results of Kuckes *et al.*[4] were reanalyzed in terms of our theory and the results are listed in Table II. Our results for other angle configurations are listed in Table III.

Kuckes *et al.* showed that if the results were plotted against the average value of T_3 over the spectrum then the data should extrapolate to the Chew-Low pole at $-\frac{1}{2}T_B$, where T_B is the deuteron binding energy. A plot of the ratios data/spectator model and FSI model/spectator model should extrapolate to unity at the pole as is shown in Fig. 4. The extrapolated cross-section

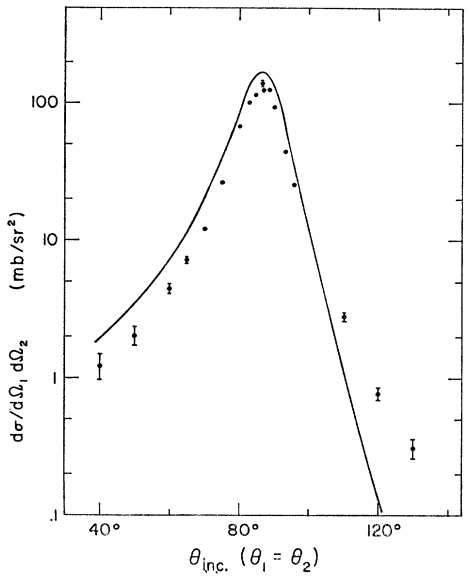

FIG. 2. Comparison of equal-angle measurements of $d\sigma/d\Omega_1 d\Omega_2$ and the spectator model; see Table I.

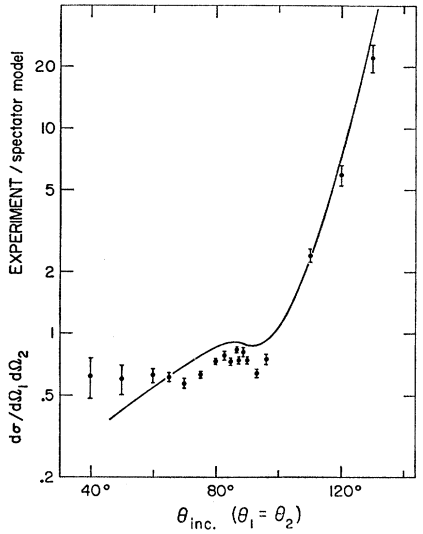

FIG. 3. Ratio of experimental value of $d\sigma/d\Omega_1 d\Omega_2$ to the spectator-model prediction. The curve indicates the ratio of the FSI model to the spectator model; see Table I.

TABLE II. 145-MeV data for $d\sigma/d\Omega_1 d\Omega_2$. The experimental results come from Kuckes, *et al.*,[a] the predictions are calculated as in the text; all cross sections are given in mb/sr². $\varphi_1=0°$ and $\varphi_2=180°$ for all configurations.

Angle (θ_1,θ_2)	Experiment	Smeared spectator model	Experiment / Spectator model	FSI model / Spectator model	$\bar{T}_3$ (MeV)
(35, 35)	12.2±0.7	21.69	0.56±0.04	0.66	3.0
(35, 40)	23.6±1.0	38.93	0.61±0.03	0.72	1.86
(35, 45)	42.6±1.7	70.36	0.61±0.03	0.79	0.95
(35, 50)	67.5±0.25	99.66	0.68±0.03	0.83	0.46
(35, 52.5)	83.6±2.7	101.84	0.82±0.03	0.84	0.43
(35, 55)	66.5±2.6	85.66	0.78±0.03	0.81	0.51
(35, 60)	27.2±1.6	42.79	0.64±0.04	0.78	1.21
(35, 65)	9.2±0.6	15.41	0.60±0.04	0.71	2.32
(30, 45)	20.6±1.3	34.87	0.59±0.04	0.70	1.56
(40, 45)	76.5±2.9	108.63	0.70±0.03	0.85	0.52
(45, 42.4)	90.2±3.1	109.19	0.82±0.03	0.86	0.49
(45, 45)	72.3±3.0	95.67	0.76±0.3	0.85	0.64
(45, 50)	33.6±1.4	45.66	0.74±0.03	0.83	1.51
(45, 55)	11.4±0.6	16.36	0.70±0.04	0.80	3.21
(45, 60)	4.8±0.4	5.21	0.92±0.08	0.95	5.53
(35, 35)	11.3±1.0	17.77	0.64±0.06	0.65	2.83
(35, 35)	14.3±1.0	22.05	0.65±0.05	0.67	3.17
(35, 52.5)	85.8±3.0	104.22	0.82±0.03	0.84	0.43
(35, 60)	27.1±1.0	42.45	0.64±0.03	0.78	1.26
(35, 65)	9.3±1.0	16.00	0.58±0.07	0.71	2.61
(45, 55)	11.9±5.0	15.24	0.78±0.04	0.80	3.11
(45, 60)	5.1±0.3	5.66	0.90±0.06	0.95	5.87

[a] Reference 4.

defect at the top of the quasifree peak, the $T_3=0$ point, is 14 and 18% at 200 and 145 MeV, respectively.

$d\sigma/d\Omega_1 d\Omega_2 dE_1$

The width of the quasifree peak in the spectrum $d\sigma/d\Omega_1 d\Omega_2 dE_1$ is characterized by the FWHM of the spectrum as a function of T_1-T_2. The results are given in Table IV and are plotted in Fig. 5. The predictions fit the data well with the FSI model preferred. The shape of the quasifree peak is seen to be a less sensitive measure of the effects of the final-state interaction than is the magnitude of the cross section $d\sigma/d\Omega_1 d\Omega_2$.

The three large included angle points in Table I showed large enhancements over the spectator model which were qualitatively described by the FSI model. The spectra $d\sigma/d\Omega_1 d\Omega_2 dE_1$ for these three configurations are shown in Fig. 6. The predictions of the spectator model and the FSI model are also shown. We estimate the natural resolution in T_1 to be 18 MeV FWHM but no attempt was made to smear the theory. The enhancements at the lower and upper ends of the T_1 spectra in

TABLE III. Non-equal-angle results for $d\sigma/d\Omega_1 d\Omega_2$. Errors quoted include normalization errors and statistical errors added quadratically. The predictions were calculated with a 30-MeV energy cutoff on T_1 and T_2. All cross sections are given in mb/sr². $\varphi_1=0°$ and $\varphi_2=180°$ unless given.

Angle (deg) (φ_1,φ_2)	Angle (deg) (θ_1,θ_2)	Experiment	Spectator model	Experiment / Spectator model	FSI model / Spectator model	$\bar{T}_3$ (MeV)
	(48, 68)	1.08±0.20	0.35	3.1 ±0.6	4.9	24.2
	(48, 60)	3.7 ±0.4	1.95	2.4 ±0.2	1.6	12.7
	(48, 48)	25.4 ±1.6	33.	0.74±0.05	0.97	2.9
	(48, 43)	70.6 ±3.3	103.64	0.68±0.04	0.90	1.09
	(48, 38.7)	129.2 ±4.7	162.47	0.80±0.04	0.90	0.61
	(48, 33)	73.0 ±3.7	100.51	0.73±0.04	0.85	1.10
	(48, 28)	29.4 ±1.6	46.00	0.65±0.04	0.75	2.06
(8.7, 171.3)	(35.7, 35.7)	5.45±1.0	8.02	0.68±0.13	0.63	7.0
(7.3, 172.7)	(43.4, 43.4)	13.8 ±1.6	16.14	0.85±0.10	0.77	4.7
(14.5, 165.5)	(43.9, 43.9)	1.82±0.43	1.40	1.3 ±0.3	1.12	7.2
(6.7, 173.3)	(48.2, 48.2)	7.85±0.99	7.00	1.12±0.14	0.92	14.8

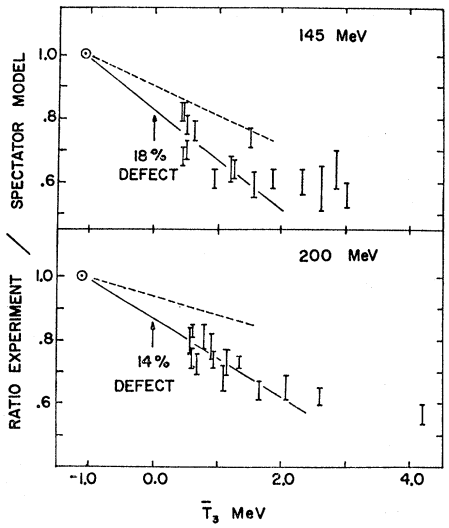

FIG. 4. Composite Chew-Low plot of 145 and 200-MeV $d\sigma/d\Omega_1 d\Omega_2$ data. The solid line indicates a linear extrapolation to the pole at $\bar{T}_3 = -1.1$ MeV drawn by eye and the dashed line is the extrapolation for the ratio of the FSI and spectator models.

the FSI theory are due to strong np final-state interactions and seem to describe the data qualitatively.

$d\sigma/d\Omega_1$

If we call the D_2 and H_2 corrected rates R_D and R_H, respectively, the total single-arm charged-particle yield is given by

$$\frac{d\sigma}{d\Omega_1} = \frac{R_D}{R_H}\frac{\rho_H N_H}{\rho_D N_D}\frac{(d\sigma/d\Omega)_{pp}}{C}.$$

Here C is the cutoff factor which corrects for the 30-MeV experimental threshold for a coincidence in either telescope. This correction was calculated using the theoretically predicted spectrum for the cross section $d\sigma/d\Omega_1 dE_1$ derived by Cromer[8] with the nucleon amplitudes mentioned above.[11]

The spectator model predicts that the total charged-particle yield is equal to the sum of the free pp and pn cross sections,

$$\frac{d\sigma}{d\Omega_1} = \left(\frac{d\sigma}{d\Omega}\right)_{pp} + \left(\frac{d\sigma}{d\Omega}\right)_{pn}. \tag{4.1}$$

When Cromer's prediction for $d\sigma/d\Omega_1 dE_1$ is integrated over the energy spectrum, the predicted cross section is equal to the spectator-model sum rule (4.1) plus an added interference term. The detected deuterons are explicitly not included and hence the previously mea-

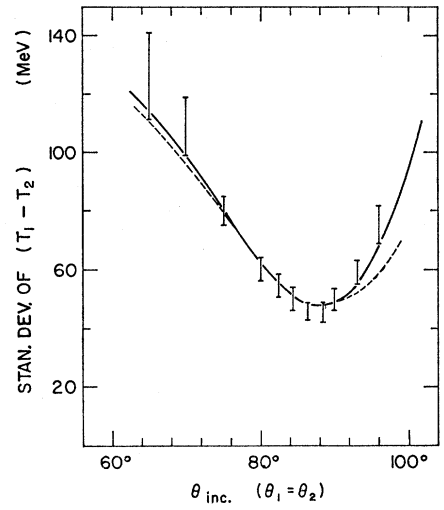

FIG. 5. Width of the spectra $d\sigma/d\Omega_1 d\Omega_2 dE_1$. The experimental values are compared with the spectator model (dashed curve) and the FSI model (solid curve); see Table IV.

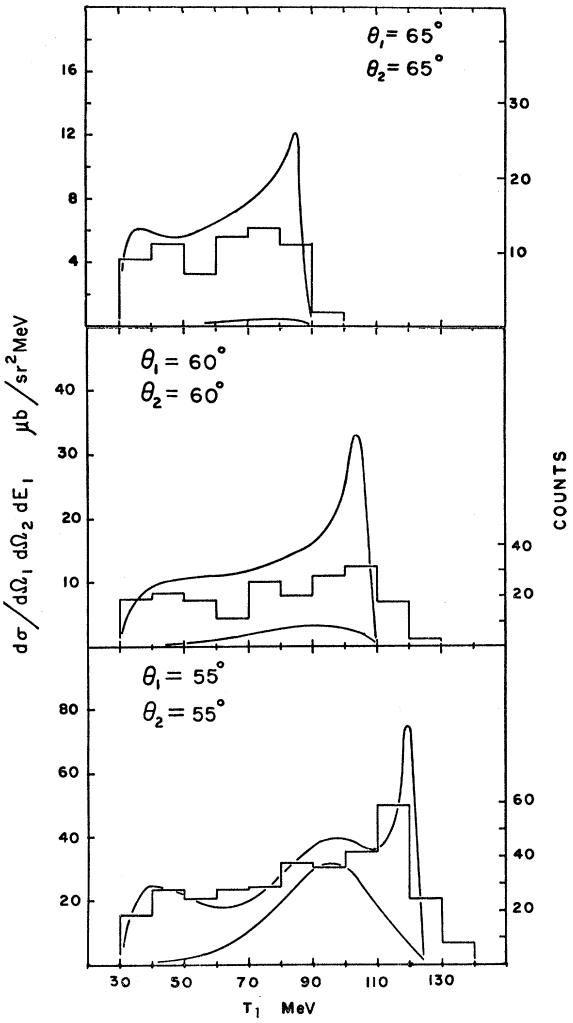

FIG. 6. $d\sigma/d\Omega_1 d\Omega_2 dE_1$ for large included angles. In each graph the histogram shows the experimental results; the lower curve is the spectator model and the upper curve is the FSI model. Experimental resolution in T_1 of about 18 MeV FWHM has not been folded into the theory.

sured deuteron yield[13] was subtracted to give the second prediction, which we also call the FSI prediction. The measured and predicted cross sections are shown in Fig. 7; the agreement is good with the simple spectator-model sum rule giving a slightly better fit.

The asymmetry of the total charged-particle yield is predicted by the spectator model to be equal to the weighted average of the pp and pn asymmetries. The predictions of the FSI model are numerically identical. The results for the asymmetry are shown in Fig. 8. Table V lists the cross-section results and Table VI lists the asymmetry results for the cross section $d\sigma/d\Omega_1$.

Singlet Deuteron

If one looks in the region of large-angle pd elastic scattering, a FSI effect referred to as the singlet deuteron manifests itself as an enhancement in the proton spectrum at one-half the energy of the elastically scattered deuterons. Data were taken at the angles $\theta_1=37°$ and $\theta_2=73.5°$, angles at which pd elastic scattering can occur with the deuteron at $T_1=112$ MeV

TABLE IV. Results for widths of $d\sigma/d\Omega_1 d\Omega_2 dE_1$. The most convenient measure of the shape of the spectra $d\sigma/d\Omega_1 d\Omega_2 dE_1$ is the FWHM of the spectra plotted as a function of the energy difference T_1-T_2. All widths are given in MeV.

Angle (θ_1,θ_2) (deg)	Experiment	Spectator model	FSI model
(32.5, 32.5)	126 ±16	111.4	114.1
(35, 35)	109 ±10	95.5	99.5
(37.5, 37.5)	79.5±5.0	78.26	79.4
(40, 40)	60.0±4.0	61.8	62.2
(41.2, 41.2)	54.5±3.7	55.3	55.4
(42.2, 42.2)	50.0±3.5	51.0	50.1
(43.2, 43.2)	45.5±2.0	48.6	47.5
(44.2, 44.2)	45.5±3.3	47.9	47.2
(45, 45)	48.5±3.0	48.8	48.7
(46.5, 46.5)	59.0±4.0	52.5	54.6
(48. 48)	75.2±6.2	57.5	69.6

TABLE V. The total charged-particle yield, $d\sigma/d\Omega_1$. All cross sections are given in mb/sr. The error quoted on the experimental measurement includes both normalization and statistical errors.

Lab angle (deg)	Experiment	Spectator model	FSI model
20	28.7±0.9	28.6	31.0
25	24.4±0.8	24.3	25.7
30	21.8±0.6	21.1	22.0
32.5	19.8±0.7	19.8	20.6
35	18.6±0.5	18.7	19.4
40	16.6±0.4	16.9	17.4
43.5	15.3±0.4	16.0	16.5
45	15.3±0.4	15.6	16.1
48	14.7±0.5	15.0	15.4
50.5	14.2±0.4	14.6	15.0
54	13.2±0.4	14.0	14.4

[13] R. E. Adelberger, thesis, University of Rochester, 1967 (unpublished).

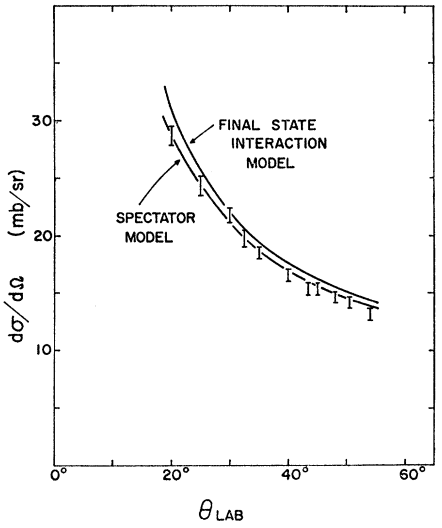

FIG. 7. The total charged particle yield, $d\sigma/d\Omega_1$. The predictions of the two models are shown; see Table V.

TABLE VI. The asymmetry of the total charged-particle yield, $d\sigma/d\Omega_1$. All asymmetries are normalized to a 100% polarized beam. The experimental error is dominated by systematic errors and is deduced from measurements of the known free pp polarization.[a]

Lab angle (deg)	Experiment	Spectator model	FSI model
20	0.383±0.01	0.40	0.42
25	0.315±0.01	0.36	0.37
30	0.224±0.01	0.28	0.28
32.5	0.17 ±0.01	0.23	0.23
35	0.12 ±0.01	0.18	0.18
37.5	0.08 ±0.01	0.13	0.13
40	0.035±0.01	0.08	0.08
42	0.00 ±0.01	0.03	0.03
43.5	−0.011±0.01	0.00	0.00
45	−0.036±0.01	−0.02	−0.02
46	−0.055±0.01	−0.04	−0.04
49	−0.09 ±0.01	−0.08	−0.08
50	−0.088±0.01	−0.09	−0.09
53	−0.115±0.01	−0.13	−0.13
54	−0.127±0.01	−0.14	−0.14
56.5	−0.143±0.01	−0.16	−0.16

[a] Reference 3.

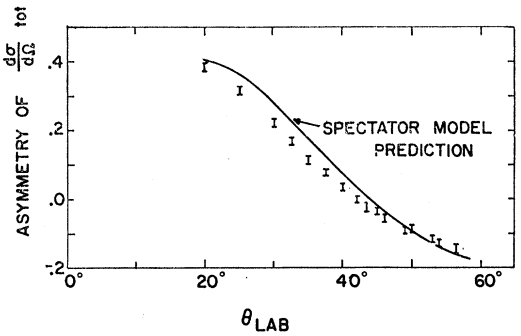

FIG. 8. The asymmetry of the total charged-particle yield. The error bars are dominated by systematic errors which were deduced by comparing measurements of pp polarization with previous measurements (Ref. 3).

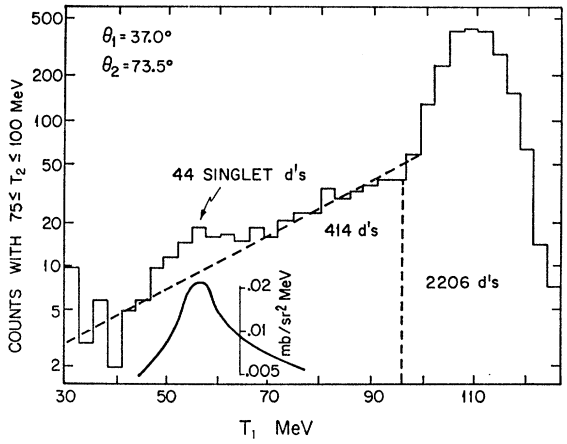

FIG. 9. Spectrum taken at $\theta_1=37°$ and $\theta_2=73.5°$ to look for the singlet deuteron. The curve shows the results of the FSI calculation without the experimental resolution folded in.

and the proton at $T_2=88$ MeV. The proton has suffered a momentum transfer of 3.3 F^{-1}, and has scattered at 105° in the pd center-of-momentum system.

We make the energy cut 75 MeV$\leq T_2 \leq$100 MeV and study the T_1 spectrum looking for an enhancement in the region $T_1 \approx 56$ MeV. The spectrum obtained is shown in Fig. 9. The spectrum shows the large *pd* elastic-scattering peak containing 2206 deuterons, an inelastic tail due to nuclear interactions in the plastic scintillator which we estimate to contain about 414 deuterons and an enhancement at the expected energy, 56 MeV, containing about 44±15 counts which we attribute to the proton member of a singlet deuteron.

To calculate the expected yield of protons in this region we used the FSI model to predict the cross section $d\sigma/d\Omega_1 d\Omega_2 dE_1$; the results are superimposed on Fig. 9. The predicted enhancement was integrated from $T_1=45$–70 MeV to give a cross section $d\sigma/d\Omega_1 d\Omega_2$ of 0.18 mb/sr². In terms of the known *pd* elastic-scattering cross section at this angle, 0.12 mb/sr,[13] the geometrical efficiency of the double coincidence for the two-body events, ϵ_{12}, and the solid angle of the first telescope, $\Delta\Omega_1$, the number of expected singlet deuteron events $R_d{}^*$ is proportional to the observed deuteron yield R_d as follows:

$$R_d{}^* = \frac{d\sigma/d\Omega_1 d\Omega_2}{(d\sigma/d\Omega_2)_{pd}} \frac{\Delta\Omega_1}{\epsilon_{12}} R_d.$$

This gives $R_d{}^*=27$ events, in fairly good agreement with observation.

The calculation of the predicted singlet deuteron yield showed that one-third of the contribution to the cross section comes from the triplet amplitude and hence the enhancement should more accurately be referred to as a slightly unbound deuteron. The magnitude of the effect seen here is consistent with previous measurements.[14] This effect, if studied more completely, could shed light on the short-range behavior of low-energy two-nucleon systems.

V. CONCLUSIONS

The impulse-approximation theory which includes the double-scattering effects in an *s*-wave low-energy approximation gives a qualitative description of the reaction $d(p,pp)n$ at 200 MeV in the region studied in the experiment. Near the quasifree *pp* scattering peak the observed cross section is about 20% lower than the spectator-model prediction and the FSI model accounts for about one-half of the defect.

The single-arm charged-particle yield is described very well by the simple sum rule (4.1). This simple sum rule is equivalent to the "area method" used in extracting *en* cross sections from *ed* scattering. Our results indicate that this sum rule fits the data much better than impulse-approximation predictions of the doubly and triply differential cross sections. *ed* scattering experiments have also confirmed this result.[15]

If one neglects the spin effects and asks what general nonpole amplitude can give the observed cross-section defect at the $T_3=0$ point, we find a 7 or 9% nonpole amplitude at 200 and 145 MeV, respectively. This amplitude probably represents the contribution of all higher diagrams except the spectator-model diagram which contributes the pole. We might expect no spin structure in the nonresonant amplitude and hence a 14 or 18% reduction in any spin observable at 200 and 145 MeV, respectively, from the spectator-model prediction. Note that it is pathologically possible for a small amplitude to cause a large change in any particular observable. Attempts to calculate such corrections, as in our FSI-model predictions, have probably only included about one-half of the nonresonant effects.[8]

ACKNOWLEDGMENTS

It is a pleasure to acknowledge the help of Rexford E. Adelberger in construction of the apparatus and the many helpful discussions with Professor Frederic Lobkowicz. The authors are indebted to Professor Alan Cromer for many helpful communications on his FSI calculations and to Professor Gregory Breit for supplying us with 200-MeV amplitudes from his phase-shift analysis YIV_{pp} and YIV_{np}.

[14] G. W. Bennett, J. L. Friedes, H. Palevsky, R. J. Sutter, G. J. Igo, W. D. Simpson, G. C. Phillips, R. L. Stearns, and D. M. Corley, Phys. Rev. Letters **19**, 387 (1967).

[15] R. Budnitz, J. Appel. L. Carroll, J. Chen, J. R. Dunning Jr., M. Goitein, K. Hanson, D. Imrie, C. Mistretta, J. K. Walker, and R. Wilson, Phys. Rev. Letters **19**, 809 (1967).